The hydration structure of aqueous carbonic acid from X-ray absorption spectroscopy

Royce K. Lam [a,b], Alice H. England [a,b,1], Alex T. Sheardy [a,b], Orion Shih [a], Jacob W. Smith [a,b], Anthony M. Rizzuto [a,b], David Prendergast [c], Richard J. Saykally [a,b,*]

[a] Department of Chemistry, University of California, Berkeley, CA 94720, United States
[b] Chemical Sciences Division, Lawrence Berkeley National Laboratory, Berkeley, CA 94720, United States
[c] Molecular Foundry, Lawrence Berkeley National Laboratory, Berkeley, CA 94720, United States

ARTICLE INFO

ABSTRACT

Despite much effort, aqueous carbonic acid (H_2CO_3) remains poorly characterized because it is very short-lived. We describe the detection and characterization of aqueous H_2CO_3 by X-ray absorption spectroscopy, wherein protonation of a bicarbonate solution continuously generates the acid under ambient conditions. Accompanying first principles calculations of the carbon K-edge transitions facilitate spectral assignment and interpretation in terms of the H_2CO_3 π^* orbital, which exhibits a small (0.2 eV), systematic blueshift relative to that of bicarbonate. These results establish the detailed hydration properties of this short-lived molecule and will thereby facilitate future studies of carbonate chemistry in biological and geological system.

© 2014 Published by Elsevier B.V.

1. Introduction

Aqueous carbonic acid (H_2CO_3) is the centerpiece of both the global carbon cycle [1–3] and physiological buffer and respiration systems [4–6], yet it remains incompletely characterized despite enormous effort. As described in a very recent review [7], carbonic acid has been well studied in both the gas phase [8–10] and in cryogenic matrixes [11–15], but there have been very few successful spectroscopic studies of the *aqueous* acid, and none of its electronic structure [16–18]. Carbonic acid is intrinsically unstable upon contact with even a single water molecule, reacting via a proton chain mechanism to rapidly form aqueous bicarbonate, carbonate, and hydrated protons [19–21], which comprises the reversible mechanism for dissolution of CO_2 gas. Here we report the first measurement of X-ray absorption spectra for aqueous carbonic acid, enabled by the use of rapid-flow liquid microjet technology [22–24], wherein protonation of a bicarbonate solution continuously generates the acid as a function of pH under ambient conditions. We combine molecular dynamics (MD) simulations with a first principles density functional theory (DFT) method [25]

to model and interpret the small (0.2 eV) measured blueshift of the carbonic acid π^* orbital in the C K-edge spectrum relative to that of bicarbonate [22], thereby gaining new and detailed insights into the nature of aqueous carbonic acid. We find that the two most stable isomers donate two strong hydrogen (H—) bonds to water oxygens and accept a stronger H-bond at the carbonyl and weaker H-bonds at the acidic oxygens, exhibiting an average hydration number of 3.17 as torsional motions rearrange the solvation structures. Because both gas phase and solid phase carbonic acid have been well studied, this work will facilitate the development of detailed models for the reversible gas-liquid chemistry of carbon dioxide.

Near edge X-ray absorption fine structure spectroscopy (NEXAFS), is an atom-specific probe of both the electronic structure of a molecule and its local chemical environment, making it a method of choice for detailed characterization of hydration interactions. Until very recently, NEXAFS studies of the carbonate system were restricted to gaseous CO_2 [26], and to carbonates adsorbed to a surface [27] or in various solid mineral forms [28] by the difficulties then inherent in addressing liquid samples by this high vacuum technology. In 2011, we reported the first NEXAFS study of *aqueous* carbonate and bicarbonate ions [22], which was followed by an X-ray emission study in 2014 [29]. In the present experiment, we follow an approach similar to that employed by Eberle et al. [16] in observing Raman spectra of aqueous H_2CO_3, enabled by the slow dehydration of carbonic acid ($k = 26.3 \text{ s}^{-1}$, $t_{1/2} = 26 \text{ ms}$) relative to the very rapid protonation rate of the
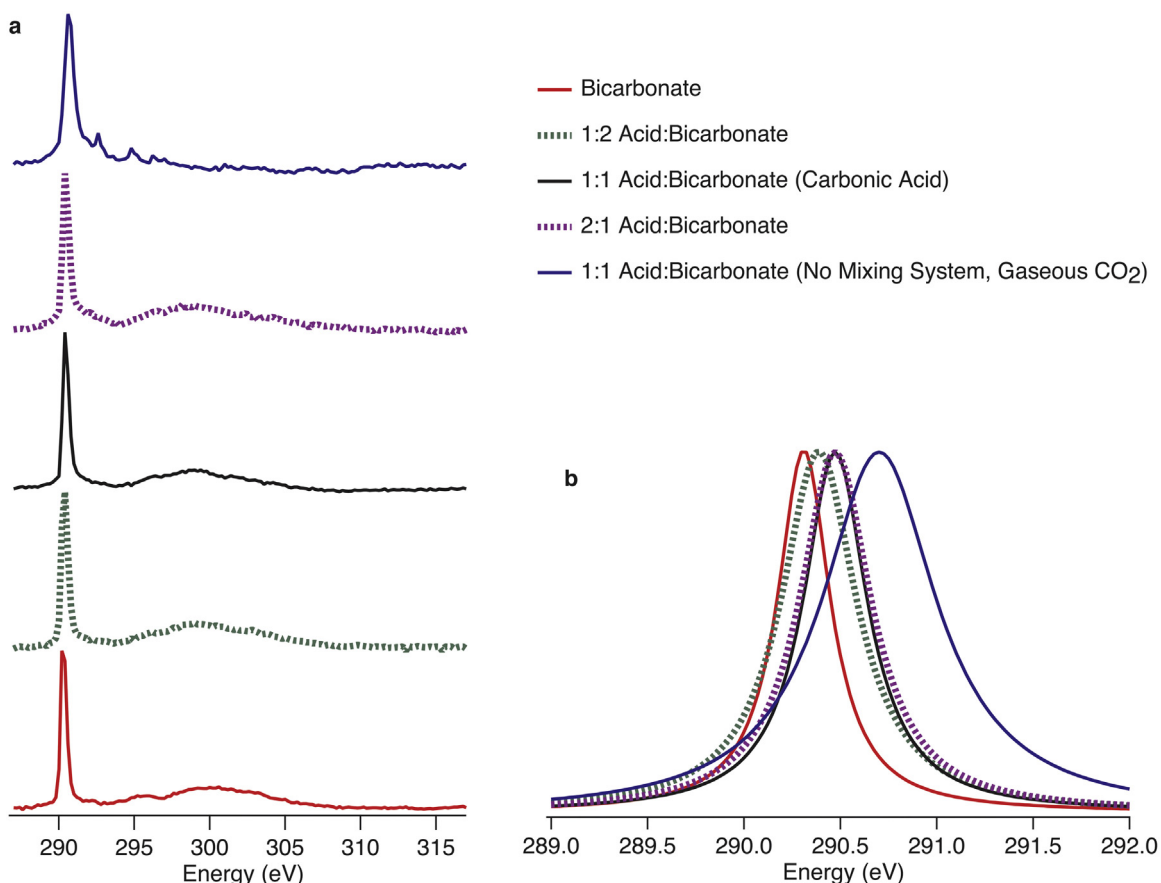

Figure 1. Peak-normalized experimental carbon K-edge X-ray absorption spectra. (a) Overview of measured spectra for bicarbonate (red), and the mixtures 1:2 HCl:NaHCO$_3$ (green), 1:1 HCl:NaHCO$_3$ (black), 2:1 HCl:NaHCO$_3$ (purple), and 1:1 HCl:NaHCO$_3$ without the mixing system (blue). (b) Lorentzian-fit experimental X-ray absorption spectra of the C(1s) → π* transition in bicarbonate (red), 1:2 HCl:NaHCO$_3$ (green), 1:1 HCl:NaHCO$_3$ (black), 2:1 HCl:NaHCO$_3$ (purple), and 1:1 HCl:NaHCO$_3$ without the mixing system (blue). The maximum absorptions are at 288.31, 288.41, 288.49, 288.49, and 288.71 eV, respectively. All other spectra were measured using a sample introduced by the rapid-flow microjet mixing system.

bicarbonate anion ($k_{on} = 4.7 \times 10^{10}$ M^{-1} s^{-1}, $t_{1/2} = 21.3$ ps) [17,30], which facilitates accumulation of carbonic acid. We combine a 0.5 M solution of NaHCO$_3$ with 1 M HCl in a high velocity liquid microjet mixing system to generate the acid at 25 °C.

2. Materials and methods

2.1. Sample preparation

Samples (0.5 M NaHCO$_3$ and 1 M HCl) were prepared using 18.2 MΩ cm resistivity water obtained from a Millipore purification system. Concentrated HCl (12.1 M) was obtained from J.T. Baker. NaHCO$_3$ with stated purity of at least 99.7% was commercially obtained from Sigma–Aldrich. Samples were used without further purification.

2.2. Experimental design

Carbon K-edge total electron yield (TEY) spectra were collected at Beamline 8.0.1. A detailed description of the experimental setup has been published previously [31]. Briefly, an intense (>10^{11} photons/s), high resolution ($E/\Delta E = 7000$), tunable soft X-ray beam is generated from an undulator at the ALS. The beam is focused (100 × 35 μm spot size) onto the liquid microjet. A dual syringe pump system (Teledyne-ISCO 260D) drives the solution through 30–50 μm inner diameter fused silica tubing to generate the liquid microjet with high linear flow velocities (1–200 m/s)

that is intersected with the X-ray beam in the high vacuum (~2 × 10^{-4} Torr) chamber.

Solutions are typically mixed shortly after the pump. The mixed solution then travels through several meters of PEEK tubing (~7.5 min mixing time) before reaching the silica capillary. The long mixing time associated with this 'standard' experimental setup precluded studies of short-lived intermediate species such as carbonic acid. To transcend this limitation, a new fast-flow microjet mixing system was designed to mix the two solutions immediately prior to the generation of the fast-flowing liquid jet. A Hastelloy Microvolume Y-Connector was mounted inside the vacuum chamber and used to generate the liquid jet. To introduce the sample, two of the openings in the connector were attached directly to the syringe pumps with PEEK tubing. The third was used to hold the silica capillary and generate the liquid jet. The mixing time in this scheme was shortened to ~0.5 ms, thereby facilitating the observation of short-lived species in solution. This time is shorter than the previously measured half-life of carbonic acid (~26 ms) [16] but significantly longer than the measured rate for the proton transfer to bicarbonate ($k_{on} = 4.7 \times 10^{10}$ M^{-1} s^{-1}) [17,30]. The liquid jet then passes through a skimmer and freezes onto a cryogenic (liquid nitrogen) trap. A TEY signal is then collected as a function of photon energy (0.2 eV step size), with a positively biased (2.1 kV) copper electrode. Vapor phase TEY spectra were measured by positioning the microjet a few microns above or below the incident X-ray beam.
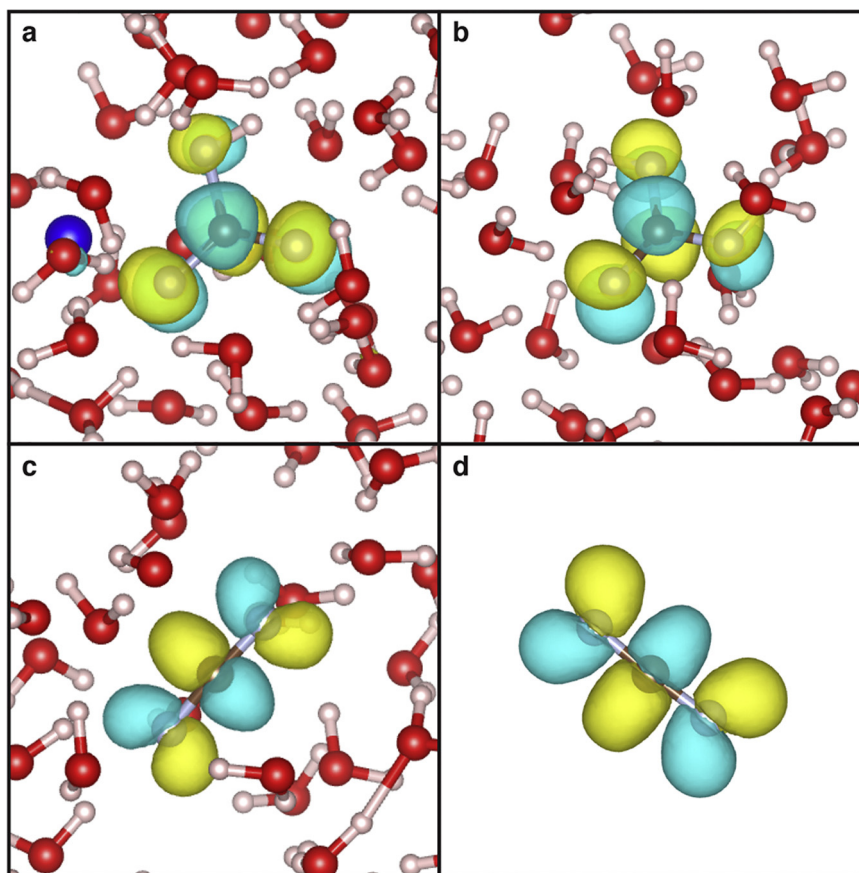
Figure 2. Isosurfaces of the core-excited electron density for π^* resonances. Oxygen atoms on the carbonate species are shaded. (a) $NaHCO_3$, (b) H_2CO_3, (c) aqueous CO_2, (d) gaseous CO_2.

2.3. Simulations and calculations

The associated molecular dynamics (MD) simulations and calculated spectra were published previously [22]. Briefly, Amber 9 [32] was used to generate 10 ns classical NVT-MD trajectories for gaseous and dissolved CO_2 and Quantum mechanics/molecular mechanics (QM/MM) trajectories for aqueous carbonate and carbonic acid. The simulation box for the aqueous species contained ~90 TIP3P water molecules. From the generated trajectories, molecular configurations were taken from 100 uncorrelated snapshots and used in the first principles spectral calculation.

X-ray absorption spectra were calculated using the excited electron and Core Hole (XCH) density field theory (DFT) method [25]. In this approach, the lowest energy core-hole excited state is treated explicitly. Higher excited states are generated from the resulting self-consistent field. The electronic structure was calculated using PWSCF from the Quantum-ESPRESSO package [33] and the exchange correlation energy was calculated with the PBE exchange correlation functional under the generalized gradient approximation [34]. A plane wave basis set with a 25 Ry kinetic energy cutoff and periodic boundary conditions was used to model the localized and delocalized states. The calculated spectra were then aligned relative to the $C(1s) \rightarrow \pi^*$ peak in the experimental gaseous carbon dioxide spectrum. Isosurfaces were calculated with Quantum-ESPRESSO and rendered in VESTA [35].

3. Results

Using the fast-flow microjet mixing system, X-ray absorption spectra of bicarbonate, 1:2, 1:1, and 2:1 mole fraction acid:bicarbonate mixtures were measured. The spectrum of 1:1 acid:bicarbonate was also measured without the high-flow mixing system, wherein the increased mixing time ensured that only gaseous carbon dioxide was present at the time of measurement. Good agreement between experimentally acquired spectra with the previously calculated [22] first principles eXcited state Core Hole (XCH) spectra [25] establish the predictive nature of the XCH method and indicate that aqueous carbonic acid is indeed the short-lived intermediate in the hydrolysis of carbon dioxide to form carbonate. Details of the hydration structure of the acid are revealed in the molecular dynamics simulations underlying the calculated XCH spectra [22].

The NEXAFS data are shown in Figure 1a. Spectra have been peak-normalized and offset for clarity. All of these experimental spectra, with the exception of that for gaseous carbon dioxide, exhibit a broad resonance between 293 and 305 eV. Through comparison with the calculated isosurfaces of excited electronic states in this energy range, this resonance is assigned to a $C(1s) \rightarrow \sigma^*$ transition for either bicarbonate or carbonic acid, depending on pH. The sharp peaks centered at ~288 eV (Figure 1b) are assigned to the respective $C(1s) \rightarrow \pi^*$ transitions for the different carbonate species. Isosurfaces for the $\pi^*(C{=}O)$ state are shown in Figure 2 for bicarbonate (Figure 2a), carbonic acid (Figure 2b), dissolved carbon dioxide (Figure 2c), and gaseous carbon dioxide (Figure 2d). These images were chosen from molecular configurations whose spectra closely matched the simulated average spectra of the thermodynamic ensembles. The experimental $C(1s) \rightarrow \pi^*$ peaks have been fit to a Lorentzian distribution (Figure 3) to facilitate the comparison with the calculated spectra. In the $C(1s) \rightarrow \pi^*$ transition, a reproducible blueshift (~0.2 eV) from the bicarbonate spectrum
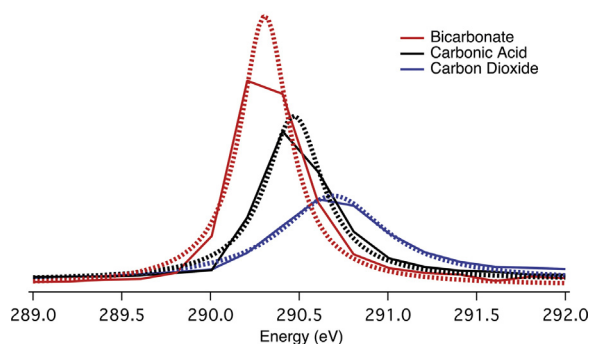
Figure 3. Unnormalized experimental spectra of the C(1s) → π* transition (solid lines) for NaHCO$_3$ (red), H$_2$CO$_3$ (black), and CO$_2$ (blue). The Lorentzian fits are shown in the dashed lines. FWHM: 0.025 eV (NaHCO$_3$), 0.038 eV (H$_2$CO$_3$), 0.11 eV (CO$_{2(g)}$).

to the 1:1 acid:bicarbonate mixture is observed. Furthermore, the gaseous carbon dioxide (1:1 mixture without the mixing system) spectrum exhibits an additional blueshift (∼0.2 eV) relative to the 1:1 mixture acquired using the fast-flow microjet mixing system. For the 1:2 acid:bicarbonate mixture, a broader C(1s) → π* peak is observed. This feature spans the width of the peaks observed in bicarbonate and in the 1:1 mixture, indicating that both bicarbonate and the species present in the 1:1 mixture were also present in the 1:2 mixture. The 2:1 acid:bicarbonate mixture produced the same shift as the 1:1 mixture.

To assign the measured spectral features to specific species, the experimentally measured spectra were compared to our [22] previously calculated spectra (Figure 4). The theoretical spectra were energy-aligned relative to the C(1s) → π* transition for gaseous carbon dioxide. Comparison of the σ* features confirmed that the species absorbing in the 1:1 and 2:1 acid:bicarbonate mixtures
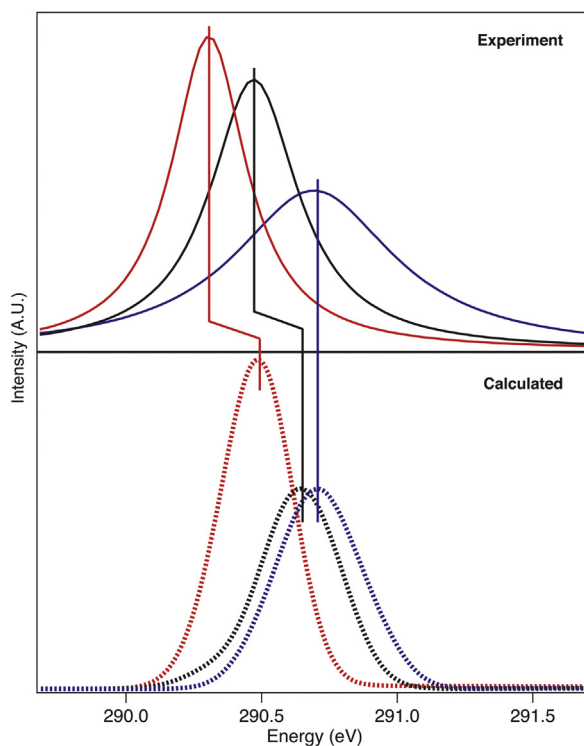

Figure 4. Lorentzian-fit experimental and calculated spectra of the C(1s) → π* transition of carbonate species. Bicarbonate (red), carbonic acid (black), and gaseous carbon dioxide (blue). Theoretical spectra were energy-aligned to the experimental spectra for gaseous CO$_2$. Experimental spectra are area normalized to facilitate comparison with the calculated spectra.

was not carbon dioxide, viz. the broad σ* resonance between 293–305 eV is present in both the experimental and theoretical spectra of bicarbonate and carbonic acid, but is not observed for carbon dioxide. Gaseous carbon dioxide does, however, exhibit a weak characteristic vibronic peak ∼2 eV higher in energy than the C(1s) → π* peak [22], which was observed in the 1:1 mixture acquired without the fast-flow mixing system. The C(1s) → π* transition observed for the 1:1 and 2:1 mixtures exhibits excellent agreement between the experiment and calculated carbonic acid spectra, viz. the reduction in peak intensity, along with the observed shifts of the π* feature is observed in both the calculated and experimental spectra. The shifts observed between different carbonate species originate from the energy differences between the ground state and core-excited states of the respective species interacting with the surrounding solvent molecules. The decrease in peak intensity of the carbonic acid feature can be attributed to the coexistence of multiple rotamers (cis–cis (CC), cis–trans (CT), trans–trans (TT)) and their respective hydration environments. In the calculated spectra for the different rotamers of carbonic acid, the C(1s) → π* features exhibit small shifts (CC: 0.024 eV blueshift, CT: 0.024 red shift relative to TT), which would effect the observed broadening and reduction in intensity. The isosurface for the cis–trans rotamer is shown in Figure 2B. The species observed in the 1:1 and 2:1 acid:bicarbonate mixtures was therefore assigned to aqueous carbonic acid. The broad C(1s) → π* peak observed for the 1:2 acid:bicarbonate mixture was attributed to the presence of both bicarbonate and carbonic acid. The agreement between the previously calculated spectrum of aqueous carbonic acid and present experimental spectra demonstrates the predictive power of our XCH spectral calculation.

The recent ab initio MD study by Kumar et al. [36] addresses the hydration of the respective carbonate species, predicting that the solvation strength correlates with the net charge on the solute, and that neutral CO$_2$ acts like a typical hydrophobic solute, inducing stronger hydrogen bonds among the adjacent waters. Considerable steric impedance to optimal solvation is observed, and hindered librational motions of the hydrogen-bonded network rearrange the solvation structures. Hydrogen bonds donated by carbonic acid to first-shell oxygen atoms are predicted to be stronger than those donated by water to either the hydroxyl or carbonyl oxygens of the acid. These predictions are partially supported by the experimental results presented here. The radial distribution functions (RDFs) for the carbonyl oxygen to water hydrogens for the different carbonate species in the snapshots used in the XCH calculations are shown in Figure 5 [37]. The shift of the first peak in the RDF to shorter distances with increasing negative charge of the carbonate species, indicative of increasing hydrogen bond strength, agrees with previous predictions [36,38,39]. In general, the increasing H-bond strength is proportional to the hydration number (measured for distances up to 2.5 Å): Na$_2$CO$_3$ (5.55), HCO$_3^-$ (4.26), H$_2$CO$_3$ (3.17), CO$_2$ (0.56). These are lower than previously reported values (9.09–5.55 for carbonate and 5.41–4.26 for bicarbonate) due to the inclusion of the sodium counterion in our simulations [22]. While the RDF for the hydroxyl oxygen to water hydrogen shown in Figure 6 also shows good agreement with the predictions made by Kumar et al., indicating that the hydroxyl oxygen of carbonic acid is a poor hydrogen bond acceptor, our simulations indicate that the H-bonds accepted by the carbonyl oxygen are slightly stronger and more structured that those donated by the hydroxyl hydrogens. This is supported by the slightly shorter =O–H$_w$ distances and the narrower first peak in the =O–H$_w$ RDF relative to that of the H$_o$–O$_w$ RDF. The structural variability observed in the H-bonds donated by the acidic protons of carbonic acid likely results from the interconversion of the carbonic acid between its different rotamers and their respective hydration environments.
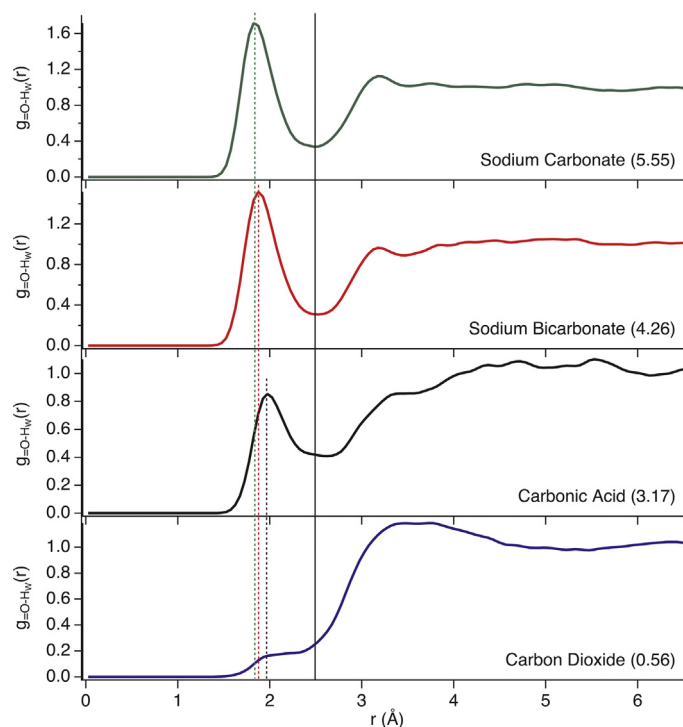
Figure 5. Calculated radial distribution functions for the carbonyl oxygen to water hydrogens of the different carbonate species. The carbonate and bicarbonate simulations include sodium counterions. Number in parentheses corresponds to the coordination number to distances of 2.5 Å.
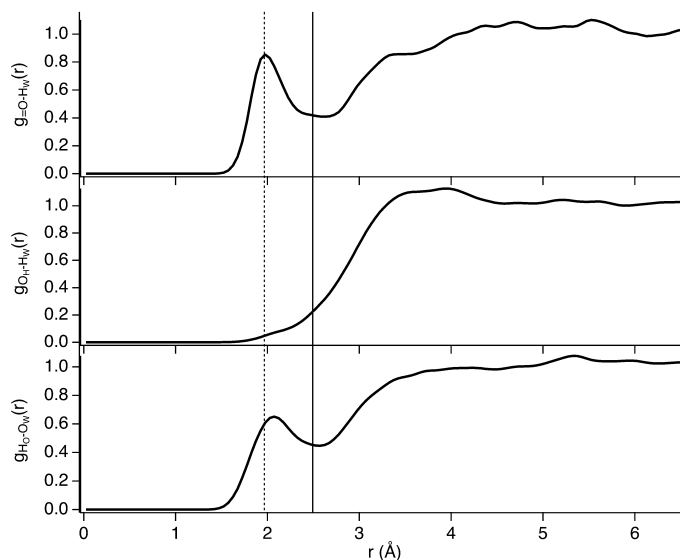

Figure 6. Calculated radial distribution functions for carbonic acid. The labels =O, O_H, and O_O refer to the carbonyl, hydroxyl oxygen, and hydroxyl hydrogen respectively. O_w and H_w refer to the oxygens and hydrogens of the water molecules.

4. Conclusions

In summary, this first characterization of carbonic acid under ambient aqueous conditions by the atom selective technique of X-ray absorption spectroscopy and first principles XCH calculations establishes the detailed hydration properties of this short-lived species. Calculated spectral energy shifts and intensities for the species observed (bicarbonate, carbonic acid, gaseous carbon dioxide) correspond well with the experimentally measured spectra, demonstrating the predictive power of the XCH technique for calculating reliable core-level spectra. We expect that these results will thereby facilitate future studies of the carbon dioxide chemistry in geological and biological systems.

References

[1] A. Putnis, Science 343 (2014) 1441.
[2] H.A. Al-Hosney, V.H. Grassian, J. Am. Chem. Soc. 126 (2004) 8068.
[3] A. Ridgwell, R.E. Zeebe, Earth Planet. Sci. Lett. 234 (2005) 299.
[4] D.N. Silverman, R. McKenna, Acc. Chem. Res. 40 (2007) 669.
[5] I. Kurtz, J. Kraut, V. Ornekian, M.K. Nguyen, Am. J. Physiol. – Ren. Physiol. 294 (2008) F1009–F1031.
[6] D.N. Silverman, S. Lindskog, Acc. Chem. Res. 21 (1988) 30.
[7] S.K. Reddy, S. Balasubramanian, Chem. Commun. 50 (2014) 503.
[8] J.K. Terlouw, C.B. Lebrilla, H. Schwarz, Angew. Chemie Int. Ed. 26 (1987) 354 (in English).
[9] T. Mori, K. Suma, Y. Sumiyoshi, Y. Endo, J. Chem. Phys. 130 (2009) 204308.
[10] T. Mori, K. Suma, Y. Sumiyoshi, Y. Endo, J. Chem. Phys. 134 (2011) 044319.
[11] M.H. Moore, R.K. Khanna, Spectrochim. Acta A: Mol. Spectrosc. 47 (1991) 255.
[12] M.H. Moore, R. Khanna, B. Donn, J. Geophys. Res. Planets 96 (1991) 17541.
[13] W. Hage, A. Hallbrucker, E. Mayer, J. Am. Chem. Soc. 115 (1993) 8427.
[14] W. Hage, K.R. Liedl, A. Hallbrucker, E. Mayer, Science 279 (1998) 1332.
[15] J. Bernard, R.G. Huber, K.R. Liedl, H. Grothe, T. Loerting, J. Am. Chem. Soc. 135 (2013) 7732.
[16] H. Falcke, S.H. Eberle, Water Res. 24 (1990) 685.
[17] K. Adamczyk, M. Premont-Schwarz, D. Pines, E. Pines, E.T.J. Nibbering, Science 326 (2009) 1690.
[18] X. Wang, W. Conway, R. Burns, N. McCann, M. Maeder, J. Phys. Chem. A 114 (2009) 1734.
[19] S. Yamabe, N. Kawagishi, Theor. Chem. Acc. 130 (2011) 909.
[20] G.A. Gallet, F. Pietrucci, W. Andreoni, J. Chem. Theory Comput. 8 (2012) 4029.
[21] M. Galib, G. Hanna, J. Phys. Chem. B 115 (2011) 15024.
[22] A.H. England, A.M. Duffin, C.P. Schwartz, J.S. Uejio, D. Prendergast, R.J. Saykally, Chem. Phys. Lett. 514 (2011) 187.
[23] M. Faubel, S. Schlemmer, J.P. Toennies, Z. Phys. D: Atoms Mol. Clust. 10 (1988) 269.
[24] K.R. Wilson, B.S. Rude, T. Catalano, R.D. Schaller, J.G. Tobin, D.T. Co, R.J. Saykally, J. Phys. Chem. B 105 (2001) 3346.
[25] D. Prendergast, G. Galli, Phys. Rev. Lett. 96 (2006) 215502.
[26] T.K. Sham, B.X. Yang, J. Kirz, J.S. Tse, Phys. Rev. A 40 (1989) 652.
[27] M. Bader, B. Hillert, A. Puschmann, J. Haase, A.M. Bradshaw, EPL (Europhys. Lett.) 5 (1988) 443.
[28] J.A. Brandes, S. Wirick, C. Jacobsen, J. Synchrotron Radiat. 17 (2010) 676.
[29] Y. Horikawa, A. Yoshida, O. Takahashi, H. Arai, T. Tokushima, T. Gejo, S. Shin, J. Mol. Liq. 189 (2014) 9.
[30] M. Eigen, Angew. Chemie Int. Ed. 3 (1964) 1 (in English).
[31] K.R. Wilson, et al., Rev. Sci. Instrum. 75 (2004) 725.
[32] D.A. Case, et al., Amber 9, San Francisco, 2006.
[33] P. Giannozzi, et al., J. Phys. Condens. Matter 21 (2009) 395502.
[34] J.P. Perdew, K. Burke, M. Ernzerhof, Phys. Rev. Lett. 77 (1996) 3865.
[35] K. Momma, F. Izumi, J. Appl. Crystallogr. 41 (2008) 653.
[36] P.P. Kumar, A.G. Kalinichev, R.J. Kirkpatrick, J. Phys. Chem. B 113 (2008) 794.
[37] A.H. England, X-ray Spectroscopy and Pulse Radiolysis of Aqueous Solutions, University of California, Berkeley, Ann Arbor, 2011, pp. 95.
[38] J.R. Rustad, S.L. Nelmes, V.E. Jackson, D.A. Dixon, J. Phys. Chem. A 112 (2008) 542.
[39] K. Leung, I.M.B. Nielsen, I. Kurtz, J. Phys. Chem. B 111 (2007) 4453.